WPMST1-CPR(17) 17333

M. Gobbin et al.

Mitigation of runaway electrons by 3D fields in ASDEX Upgrade

Preprint of Paper to be submitted for publication in Proceeding of 44th European Physical Society Conference on Plasma Physics (EPS)

This work has been carried out within the framework of the EUROfusion Consortium and has received funding from the Euratom research and training programme 2014-2018 under grant agreement No 633053. The views and opinions expressed herein do not necessarily reflect those of the European Commission.

Runaway electron mitigation by 3D fields in the ASDEX-Upgrade experiment

M.Gobbin[1], L.Li[2], Y.Q.Liu[3], L.Marrelli[1], M.Nocente[4], G.Papp[5], G.Pautasso[5], P.Piovesan[1], M.Valisa[1], D.Carnevale[6], B.Esposito[7], L.Giacomelli[8], M.Gospodarczyk[6], P.J.McCarthy[9], P.Martin[1], W.Suttrop[5], M.Tardocchi[8], M.Teschke[5], the ASDEX Upgrade Team[5] and the EUROfusion MST1 Team*

[1] *Consorzio RFX, Padova (CNR, ENEA, INFN, Universitá di Padova, Acciaierie Venete SpA)- Italy*

[2] *College of Science, Donghua University, Shanghai, Peoples Republic of China*

[3] *General Atomics, San Diego, CA 92186-5608, USA*

[4] *Dipartimento di Fisica, Universitá di Milano-Bicocca, Milano, Italy*

[5] *Max-Planck-Insitute for Plasma Physics, Garching, Germany*

[6] *Dip. di Ing. Civile ed Informatica, Universitá di Roma Tor Vergata, Italy*

[7] *ENEA, Fusion and Nuclear Safety Department, Via E. Fermi 45, 00044 Frascati, Italy*

[8] *CNR-IFP, Milan, Italy*

[9] *Department of Physics, University College Cork, Cork, Ireland and*

∗see H. Meyer et al., Nuclear Fusion FEC 2016 Special Issue (2017)

Disruption-generated runaway electron (RE) beams represent a severe threat for tokamak plasma-facing components in high current devices like ITER, thus motivating the search of mitigation techniques. The application of 3D fields might aid this purpose and recently was investigated also in the ASDEX Upgrade experiment by using the internal active saddle coils (termed B-coils). Resonant magnetic perturbations (RMPs) with dominant toroidal mode number $n = 1$ have been applied by the B-coils, in a RE specific scenario, before and during disruptions, which are deliberately created via massive gas injection. The application of RMPs seemingly changes the dynamics of the disruption and results in a significantly reduced current and lifetime of the generated RE beam. A similar effect is observed also in the hard-X-ray (HXR) spectrum, associated to runaway electron emission, characterized by a partial decrease of the energy content below 1MeV when RMPs are applied. The strength of the observed effects strongly depends on the upper-to-lower B-coil phasing, i.e. on the poloidal spectrum of the applied RMPs, which has been reconstructed including the plasma response by the code MARS-F. A crude vacuum approximation fails in the interpretation of the experimental findings: despite the relatively low β ($< 0.5\%$) of these discharges, a modest amplification (factor of 2) of the edge kink response occurs, which has to be considered to explain the observed suppression effects.

PACS numbers:

I. INTRODUCTION

The mitigation of runaway electrons still represents an important challenge in the development of a tokamak fusion reactor and in particular for future operations in ITER [1]. These high energy particles are often generated during disruptions [2–4], large scale macroscopic events in tokamak plasmas that lead to a rapid termination of the discharge. During disruptions the machine is subjected to massive thermal and electromagnetic loads as the thermal energy and current dissipate in a time on the order of few milliseconds. The temporal sequence for these highly deleterious phenomena are often characterized by a precursor phase during which the plasma pressure and current build up to conditions that trigger MHD instabilities followed by the loss of the thermal energy to the first wall (thermal quench). Finally, the ohmic current rapidly falls to zero inducing huge electromechanical forces on plasma facing components (current quench phase). Due to the fast growth of the toroidal electric field during the current quench phase, a fraction of electrons may be continuously accelerated up to velocities close to the speed of light i.e. they undergo a runaway process. Indeed, runaway electrons are generated when the force exerted on the free electrons by the toroidal electric field exceeds the frictional drag due to collisions with the background distribution of electrons (primary RE production) [5]. Moreover, if a runaway electron is subject to a Coulomb collision with a thermal one, the latter may gain enough forward momentum to become, in turn, a runaway. Thereafter, by the same process, both electrons can create even more runaways (secondary RE or avalanche generation [6]).

Thus, RE generation depends both on the applied electric field and on collisionality i.e. the plasma density; if no other RE energy loss mechanisms other than collisional damping are involved, a simple relation holds between the critical value of the electric field (in V m^{-1} units) necessary to produce any runaway and the electron density n_{20} in units of 10^{20} (m^{-3}) [7]:

$$E_{crit} = \frac{n_e e^3 \ln(\Lambda)}{4\pi\epsilon_0 m_e c^2} \approx 0.08 n_{20}. \tag{1}$$

In standard discharges the loop voltage is small and thus the corresponding electric field is below E_{crit}; nevertheless the large electric field generated during disruption events can accelerate the electrons up to energies greater than 10 MeV and the plasma resistive current is replaced by a current of relativistic electrons. In ITER the secondary RE generation will be dominant and significantly different from those experimentally observed up to now; thus an adequate protection plan for ITER is difficult to extrapolate and to be validated in existing tokamaks [8, 9]. Theoretical calculations predict that the avalanche process could multiply the number of relativistic electrons

by about twelve orders of magnitude more in ITER than in JET [10]. Most of the post-disruption current is expected to be carried by runaway electrons with an energy up to $\sim$ 100 MeV [11]. These energetic particles can strike and seriously damage the surrounding structures through their highly localized energy deposition. The prevention and mitigation of their harmful effects is thus of paramount importance to ensure a long life to a commercial reactor. For safe operations in ITER the post-disruption runaway current must be kept much below 1MA and the current quench phase duration between 50ms and 150ms [12].

The main strategies envisaged to mitigate post-disruption generated runaway electrons are based on:

1. methods to increase the plasma density, in order to enhance the critical electric field;

2. deconfinement techniques which reduce the RE loss time;

3. magnetic confinement of the RE current while energy is removed by loop voltage control.

While the methods 1) and 2) act in order to suppress the primary RE generation and avalanche mechanism, the third is based on the runaway beam position control [13, 14]. At present the first one, i.e. the dissipation of the energy of fast electrons via Coulomb scattering by increasing the density, is considered to be the main solution. Several techniques directed to this end are extensively investigated in the tokamak community, for instance Massive Gas Injection (MGI) [15–20] and shattered pellet injection [21, 22].

RE suppression by deconfinement takes advantage of magnetic perturbations to keep magnetic surfaces from healing. This can be obtained both by producing secondary disruptions by dense gas jets injected repeatedly during the CQ phase [23] or by applying external non axi-symmetric fields generated by external coils. In particular this latter approach [24, 25] has been tested in existing devices [26–30] and examined with numerical simulations dedicated to ITER scenarios [11, 31, 32]. In these experiments, resonant magnetic perturbations (RMPs) [33] could decrease the post-disruption RE current if quickly switched on prior to RE generations with an efficiency depending on their amplitude. Nevertheless, a systematic suppression of runaway electrons has not yet been achieved [27] and also the results obtained from RMPs with different toroidal/poloidal wave numbers [28] require further investigation.

A major and innovative contribution to these studies [34] comes from the experiments recently performed in the medium size tokamak ASDEX Upgrade [35], here discussed in detail. RMPs applied by external coils [36] before disruption events have been found to significantly reduce the current

and lifetime of the resulting RE beams with a strength depending on the perturbation poloidal spectrum. Such a phenomenology has been explained by evaluating the total radial magnetic field taking into account the plasma response [37] to the RMPs i.e. the capability of a plasma, close to marginal stability, to amplify magnetic perturbations and hence to experience significant helical deformations. Indeed, a vacuum approximation fails in the interpretation of the experimental data.

In the next section of the paper the baseline runaway scenario in ASDEX Upgrade and the phenomenology of standard discharges, when no perturbations are applied, is presented. Section III reports the effect of RMPs with different poloidal spectrum on the final runaway current. The impact of RMPs on the disruption dynamic, on the thermal quantities and HXR radiation are described in Sections IV-VI. The interpretation of the experimental results by considering the role played by the plasma response to RMPs is illustrated in Section VII. Finally, the effect of magnetic perturbations of reduced amplitude or applied only during the post-disruption phase is investigated in Section VIII. The conclusions are drawn in the last section.

II. RUNAWAY SCENARIO IN ASDEX UPGRADE

AUG disruptions, typically of diverted and elongated plasmas, do not exhibit formation of RE beams. Indeed, usually a disrupting plasma has a density large enough to suppress the RE primary generation and avalanche mechanisms are not expected to be significant in AUG; moreover, during the thermal quench, an elongated plasma becomes vertically unstable, moves up or downwards, becomes limited on the lower or upper divertor and develops a region of open flux surfaces (halo) from which the REs escape within milliseconds. Therefore, in order to allow studies of RE generation and mitigation during disruption a dedicated scenario has been established [19].

The ASDEX Upgrade scenario for these experiments is based on a discharge with toroidal magnetic field $B_T = -2.5$ T, plasma current of $I_p = 800$ kA and central electron density in the range: $2.5 - 3.5 \cdot 10^{19}$ m^{-3} [19, 38]. The plasma is circularly shaped (Fig.1-(e)), limited by the inner wall; a power of 2.5 MW of Electron Cyclotron Resonance Heating (ECRH) is applied for 100 ms from $t = 0.9$ s to heat the plasma and introduce a fast particle seed just before the disruption, which is triggered by the injection of argon gas ($1.7 - 5 \cdot 10^{21}$ atoms) at $t = 1$s. The injected argon induces a fast quench of the current driven by thermal electrons, followed by a long-lived runaway beam with a toroidal current up to 400kA and lasting up to 500ms. The RE beams are reproducible but changes in the current ramp up history, in the toroidal magnetic field, in the

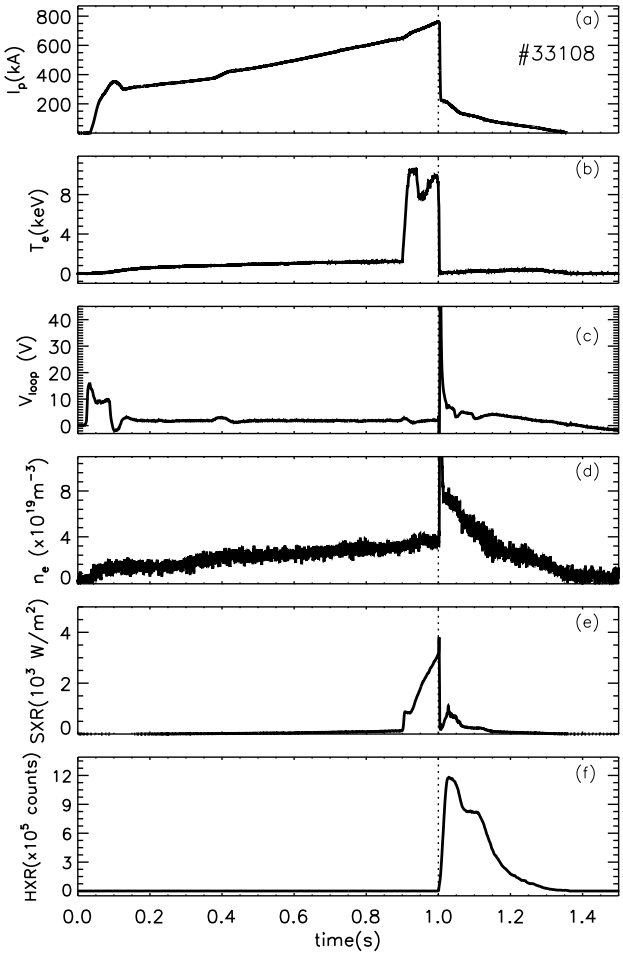

FIG. 1: Evolution of (a) plasma current, (b) core electron temperature (ECE at $R = 1.67$m,$Z = 0.024m$), (c) loop voltage (MAU-ULid12 signal), (d) electron density at the edge (along H-5 chord), (e) SXR brightness (along line of sight F017 of tomography camera F) (d) HXR emission for the shot #33108 ($LaBr_3$(Ce) scintillator diagnostic). The dashed vertical black line at 1s corresponds to the trigger time of disruption.

deposited ECRH power, in the reference current imposed by the control system might prevent the formation of a beam or influence its current and duration. The variation of these conditions must be further exploited and extended.

Fig.1 shows the main waveforms for a typical discharge evolution; the plasma current I_p is ramped till $t = 1$ s, when the disruption is induced. Then, part of I_p is converted into runaway beam current (I_{RE}) with an initial value of $\sim$ 200 kA decreasing to zero in about 0.35 s. The

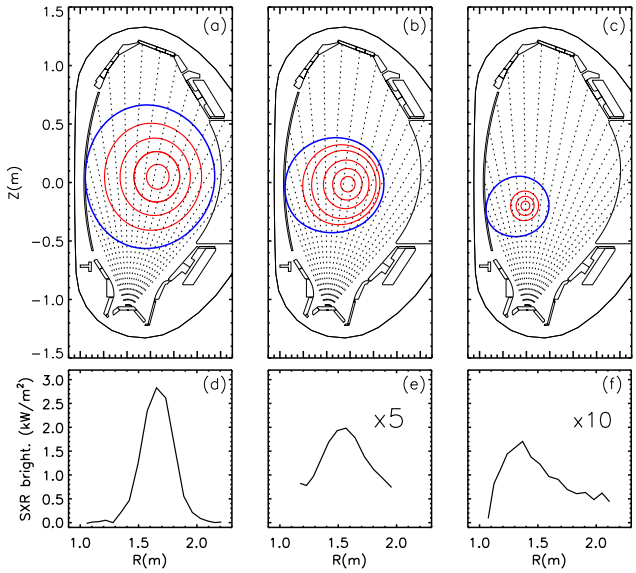

FIG. 2: Reconstruction of plasma equilibria at three different times for the shot #33108: panel (a) for t=0.98s, panel (b) for t=1.1s, panel (c) for t=1.2s. The dotted lines are the chords of the soft-X-ray tomography camera F. In (d),(e),(f) the associated soft-X-ray radiation as observed from the soft-x-ray tomography camera F.

ramp down of the current is operated by the control system following a pre-programmed time trace. When larger amounts of argon are injected, the current decay is accelerated and the Ohmic system cannot keep the actual current at the level of the reference value. The central electron temperature measured by the Electron Cyclotron Emission diagnostic grows from 1 to $\sim$ 10 keV during the ECRH heating and collapses at 1 s in less than 1 ms (thermal quench phase, in panel (b)). Before the disruption the loop voltage is below $3V$ but fast increases during the current quench up to $\sim 20V$; then, it decreases again to values around $5V$ in the RE beam phase and finally to zero. Panel (d) shows the electron density n_e along an interferometer chord at the edge of the plasma; when argon is injected the density sharply grows by about a factor of ~ 3; then during the RE beam phase it is reduced from $8 \cdot 10^{19} m^{-3}$, just after the disruption, to zero. In general the argon puff might increase the density of a factor between 2 and 6. The soft-X-ray radiation from the core of the plasma is reported in panel (e); it basically follows the electron temperature evolution: a fast growth during the ECRH heating and a sudden collapse at the thermal quench phase. Finally, Hard X-Ray (HXR) measurements from a scintillator diagnostic [39, 40] are reported in the last panel; they are greater than zero only in the post-disruption phase with a temporal evolution similar to the plasma current in panel (a).

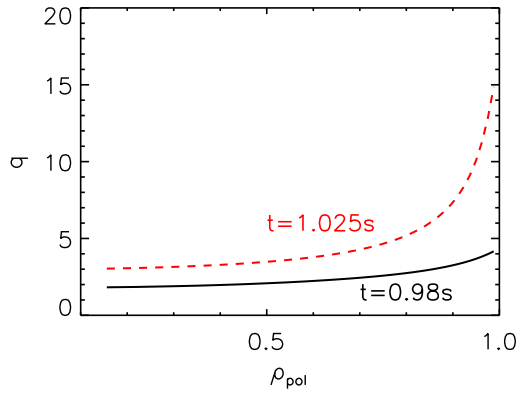

FIG. 3: Safety factor profile as function of the normalized square root of poloidal flux before ($t = 0.98s$, black solid line) and after the disruption ($t = 1.025s$, red dashed line) for the shot #33108.

The evolution of the plasma equilibrium before and after the disruption is shown in Fig.2 for three times: $t = 0.98$s (a), $t = 1.1$s (b) , $t = 1.2$s (c); panels (d)-(e)-(f) display the corresponding SXR profiles along the lines of sight plotted with dotted lines in (a)-(b)-(c). A good agreement is found between the reconstructed equilibria and the SXR profiles. Before the disruption the average minor radius of the plasma is $a \sim 0.53$m with a major radius of $R_0 = 1.63$m. Then, 100ms after the disruption, the plasma has moved inward and its minor radius is reduced to $a \sim 0.4$m; the associated SXR radiation is decreased by a factor 5. Finally, during the later stage of its evolution, at $t = 1.2$s the RE beam plasma minor radius if further lowered to $a \sim 0.2$m with SXR radiation reduced by a factor 10 with respect to $t = 0.98$s.

The pre-disruption safety factor profile ($q = rB_T/B_P R_0$ with B_T,B_P the toroidal and poloidal field respectively and r,R_0 the minor and major radius of the plasma) at $t = 0.98s$ is shown in Fig.3 (black solid line) as function of the square root of the normalized poloidal flux; at the edge $q(a)$ is slightly greater than 4. An example of q profile corresponding to $25ms$ after the disruption is reported in the same Fig.3 with a dashed red line characterized by values at the edge up to 15. Due to the decrease of the minor and major radius towards the end of the beam lifetime, lower values of the edge safety factor are expected in this later phase ($t > 1.2s$), in the range $q(a) \sim 5-8$ or lower.

III. APPLICATION OF MAGNETIC PERTURBATIONS BY B-COILS

ASDEX Upgrade is equipped with a set of sixteen non-axisymmetric in-vessel coils in the form of two toroidal rows of eight coils (termed B-coils) above and below the tokamak midplane on the outer side of the torus (low field side). During the experiments described in this paper, they were powered by independent power supplies which produce a radial field of $\sim 10^{-3}$ T at the plasma boundary in front of an upper coil ($b^r/B_T \lesssim 10^{-3}$ for typical 2.5T operations). The B-coils can generate resonant magnetic perturbations with dominant toroidal mode numbers $n = 1, 2, 4$. The poloidal mode number spectrum m is defined by the poloidal dimension of the coils and their reciprocal distance; generally there is no single corresponding m, but a broad spectrum of modes and harmonics. The differential phase $\Delta\phi$ between the current harmonic flowing in the upper ($I_{\rm upper}$) and lower ($I_{\rm lower}$) set of coils can be modified in order to change the alignment of the perturbation field with respect to the equilibrium magnetic field lines and hence the degree of MP resonance with rational q surfaces. The differential phase $\Delta\phi$ is defined through the following relations: $I_{\rm upper} \propto \cos(n\phi_{\rm coil})$ and $I_{\rm lower} \propto \cos(n\phi_{\rm coil} + \Delta\phi)$ where $\phi_{\rm coil}$ is the toroidal angle location of the center of a B-coil. One-side effect of the plasma response to the field perturbations may be a modification of these resonance conditions with respect to a vacuum approximation.

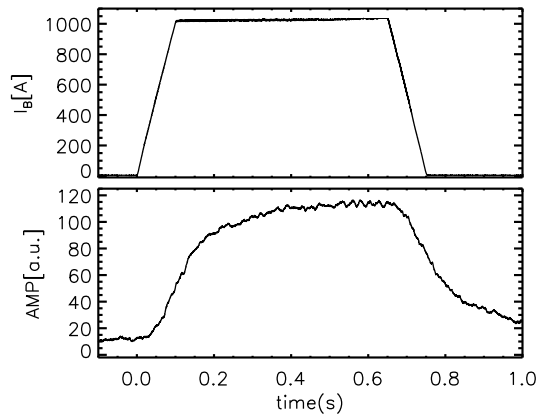

FIG. 4: Upper panel: waveform for the current flowing in one of the B-coil (MAW-IBu1 signal); lower panel: corresponding field in the plasma estimated from high field side probe coils (from shot #33706, the time scale is shifted of $-0.5s$ with respect to the experimental one, so $t = 0$s coincides with the time at which the B-coil are turned on).

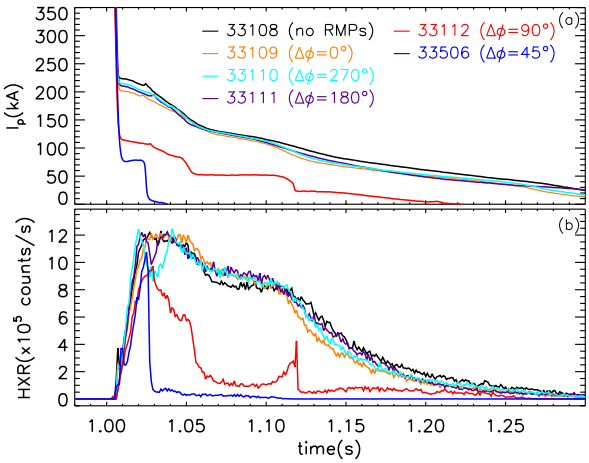

FIG. 5: (a) Plasma current during the post disruption phases for different values of $\Delta\phi$ and (b) corresponding HXR emission from $LaBr_3(Ce)$ scintillator.

In the experiments reported here a scan of $\Delta\phi$ in steps of 45° is performed and the perturbations are characterized by a dominant $n = 1$ toroidal mode number; a toroidal field of $2.5T$ limits the maximum current in the B-coils to $I_B = 1$ kA. The total perturbation field requires hundreds of milliseconds to build up in the plasma region, because of surrounding conducting structures as can be observed in Fig.4. The upper panel shows the current flowing in one of the coils, while the lower one an estimate of the field evolution inside the plasma as measured by large coils located in the high field region (SAT coils). The current is turned on at $t = 0$s, but only after ~ 300ms the field in the plasma reaches its maximum value; even to reach half of the maximum about 150ms are required. These times are comparable with the RE beam lifetime; this is why perturbations have been initially applied from $0.5s$ before the disruption. Some experiments with the RMPs applied from a time following the disruptions have been also executed and are reported in Section VIII. Here and in Sections III-VII only discharges with perturbations pre-existing the disruption are considered. These experiments are still of general relevance, since in large machines operated at high magnetic field like ITER, a perturbation preceding the disruption might be useful to prevent the formation of huge RE beams difficult to mitigate with standard methods. Clearly, such an approach requires disruption prediction methods currently in development and investigation [41–44].

A differential phasing scan between the top and bottom coil set was carried out using the same ramp-up and gas injection scenario; the results for the RE current and HXR radiation are reported in Fig.5. Panel (a) shows that both the initial runaway current and the beam duration in the

post-disruption phase are almost halved with respect to the unmitigated RE discharge without external field application when $\Delta\phi = 45°, 90°$. Similarly, the HXR signal decreases by a factor of $\sim 2-3$ in less than 70 ms, and remains close to zero afterwards.

This phenomenology is not observed for other differential phases of the B-coils; no significant effect of the applied perturbation is visible for $\Delta\phi = 0°, 180°$ and 270°, only in the first case a very slight reduction of the current with respect to the unperturbed current waveform occurs but without any important decrease of the HXR emission and within the statistical variation of standard unperturbed discharges. On the other side, the discharge reported in this plot with $\Delta\phi = 90°$ is characterized by a reduction of the RE current ($\sim -40\%$) and HXR emission ($\sim -60\%$). This behaviour is even more pronounced for $\Delta\phi = 45°$, where the runaway beam initial current is much lower than in the other discharges (~ 70 kA). It is worth to note the presence of sudden drops in the current waveforms for $\Delta\phi = 45°, 90°$ correlated with spikes in the HXR signal, a signature of abrupt RE losses.

In the next three sections the main features of shots with RMPs will be discussed with respect to disruption dynamic, thermal quantities and hard-X-ray radiation.

IV. EFFECT OF RMPS ON DISRUPTION DYNAMICS

External $n = 1$ fields partially affect the disruption dynamic, as reported in this Section. Indeed, shots with $\Delta\phi = 45°, 90°$ RMP are characterized by a different evolution during the current quench phase after the disruption and in the RE beam decay rate. For this analysis the I_p current waveform during the quench phase, between the maximum value and the beginning of the RE plateau, has been interpolated by an exponential fit:

$$\frac{I_p}{I_{CQ}} = e^{-\frac{t-t_{CQ}}{\tau_{CQ}}} \tag{2}$$

where I_{CQ} is the current at $t = t_{CQ}$ and τ_{CQ} defines a characteristic current quench time which is inversely proportional to the I_p decay rate. Lower τ_{CQ} are thus associated to faster decrease of the plasma current after the disruption. As reported in Fig.6-(a), those shots which significantly reduce the initial RE beam current generally have $\tau_{CQ} < 2.3$ms while most of the others range between this value up to 3.2ms. Both the shots with $\Delta\phi = 45°$ (blue circles) are characterized by values of τ_{CQ} among the lowest ones. For shots with $\Delta\phi = 90°$ (red diamonds) the dispersion is greater but still roughly scale with the final runaway beam current. Also in past experiments in DIII-D a similar phenomenology was observed [45]; there, in particular, discharges with RMPs

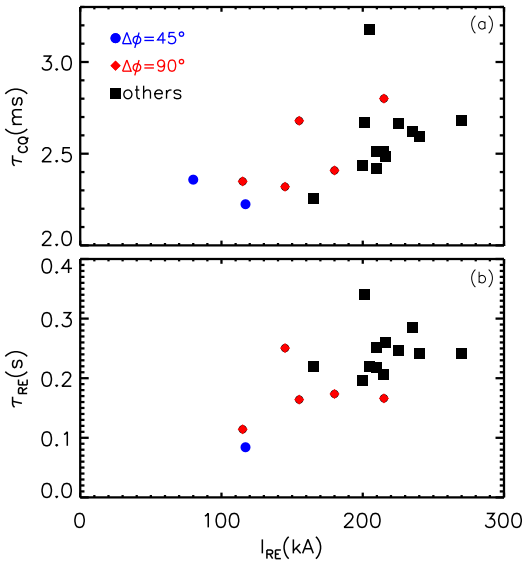

FIG. 6: Current quench (a) and runaway beam (b) decay time as function of the final post-disruption RE current.

application were characterized by current quench decay rates among the highest ones. These facts have been interpreted as a general worsening of the confinement properties when perturbations are applied. Here, in particular, RMPs with $\Delta\phi = 45°, 90°$ might enhance the MHD activity and/or create partially chaotic regions leading to a faster degradation of the thermal confinement and thus to a sudden increase of the plasma resistivity which in turn determines a more rapid current quench.

The characteristic runaway beam current decay time τ_{RE} has been estimated by a lineat fit:

$$\frac{I_p}{I_{RE}} = 1 - \frac{t - t_{RE}}{\tau_{RE}} \tag{3}$$

where t_{RE} is the time at which the RE beam plateau begins and, as usual, I_{RE} is the corresponding current. The results are reported in Fig.6-(b) with τ_{RE} vs I_{RE}. Most of the shots with the most efficient perturbations ($\Delta\phi = 45°, 90°$, blue circles and red diamonds) are characterized by significant reduced values of τ_{RE}, lower than $0.2s$. All the RE beams in shots without RMPs or with $\Delta\phi \neq 45°, 90°$, on the contrary, have a slower decay with τ_{RE} between 0.2s and 0.4s. It is worth noting that one of the shot with $\Delta\phi = 45°$ is not reported in this plot since it was affected by a fast loss of position control.

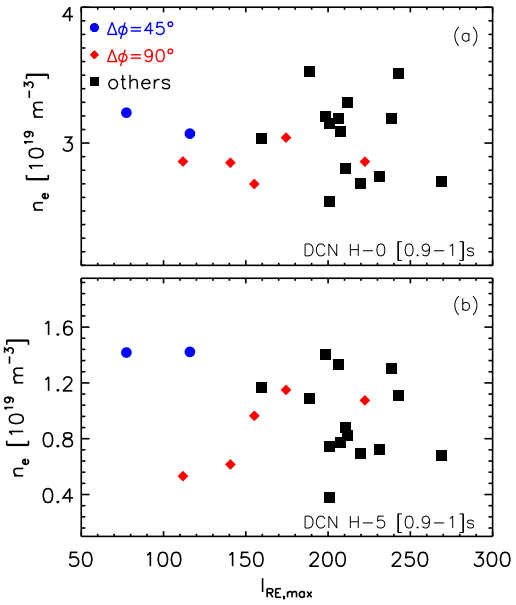

FIG. 7: (a) Core (H-1 chord) and (b) edge (H-5 chord) electron density before the disruption (averaged between $0.9 - 1s$) as function of the post-disruption runaway current.

V. IMPACT OF RMPS ON THERMAL QUANTITIES

The application of perturbations is correlated to a different behavior of the main thermal quantities, like electron density and temperature, with respect to unperturbed shots. Fig.7 shows the density averaged in the time interval $0.9 - 1.0s$ for an interferometer chord passing through the core of the plasma (panel (a)) and for an other one closer to the edge region (panel(b)) as function of the final post-disruption runaway current I_{RE}. A clear difference between shots with $\Delta\phi = 45°, 90°$ and other cases is not visible and the density spans between 2.5 and $3.5 \cdot 10^{19} m^{-3}$ in the core and between 0.4 and $1.6 \cdot 10^{19} m^{-3}$ at the edge. In this latter case the discharges with $\Delta\phi = 45°$ perturbations (blue circles) are among those with higher density but these values are also common to other shots which do not affect significantly the final runaway current. Moreover, when $\Delta\phi = 90°$, I_{RE} decreases at larger densities. In order to highlight the role played by perturbations on density, the same data of Fig.7 have been reported also in Fig.8 but as function of the phasing $\Delta\phi$; the average density for the unperturbed shots is represented by the dotted line (with a standard deviation of $\sim 0.5 \cdot 10^{19} m^{-3}$). In the core region (panel (a)) a partially higher density is found for phasing of $0°, 45°, 270°$; such a behavior becomes more pronounced at the edge of the plasma (panel (b)) where most of the shots with perturbations applied are characterized by an increased density with respect to the average of standard discharges. These plots suggest that the

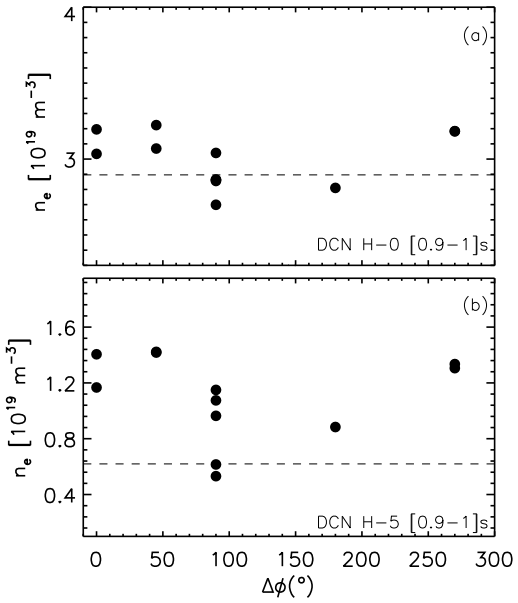

FIG. 8: (a) Core (H-1 chord) and (b) edge (H-5 chord) electron density before the disruption (averaged between $0.9 - 1s$) as function of the perturbation phasing.

presence of perturbations might be correlated to an enhanced plasma-wall interaction but that is not responsible of the mitigation effect on runaways. Indeed, panel (b) of Fig.7 and 8 clearly state that the perturbation effect on density is not correlated with their efficiency in reducing the final runaway beam current. For instance those shots with $\Delta\phi = 270°$ and $\Delta\phi = 45°$ are characterized by a similar density but only the latter successfully reduce I_{RE}. On the contrary, there are shots with $\Delta\phi = 90°$ significantly affecting the runaway current with density closer to those typical of standard shots. Thus we can conclude that the mitigation effect of RMPs on runaways is not a mere consequence of different density regimes induced by the applied perturbations before the disruption.

The electron temperature profile measured by ECE diagnostic follows the same evolution during the time interval $0 - 0.9s$ regardless of the RMPs application. Nevertheless, during the last 100ms when ECRH is applied, the T_e profile of discharges with $\Delta\phi = 45°$ are characterized by a region of lower temperature. This can be appreciated in Fig.9-(a) reporting $T_e(R)$ profiles averaged both in time (during $0.9 - 1$s) and over more shots. The black (squares) line refers to unperturbed discharges while the blue line (circles) to those with $\Delta\phi = 45°$. While the profiles are very similar in the core region and near the edge, between $R = 1.8$m and $R = 2.0$m an important difference appears. Something of analogous, but of smaller extent, is observed also when $\Delta\phi = 90°$ (red line

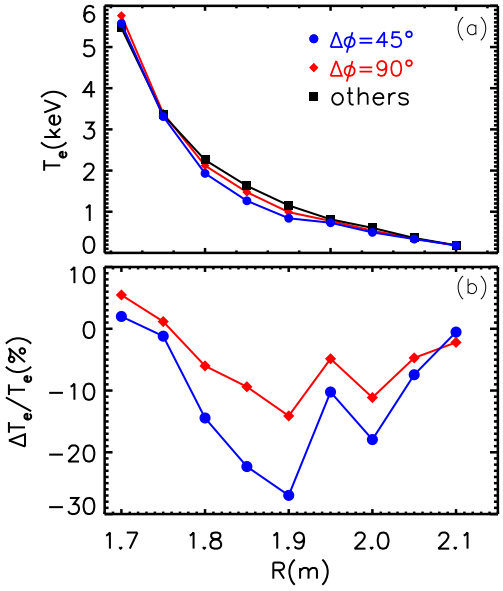

FIG. 9: Averaged electron temperature profiles (a) and percentage variations with respect to unperturbed discharges (b) in the time interval $0.9 - 1$s.

or diamonds). In panel (b) of the same figures the percentage deviation of temperature ($\Delta T_e/T_e$) from the standard cases is plotted both for $\Delta\phi = 90°$ and $\Delta\phi = 45°$; while in the former case such a deviation is limited below the $\sim 10\%$, for the latter it can increase up to 30% around $R = 1.9m$ corresponding to an absolute reduction in temperature also of 400eV.

Since the core temperatures are almost unchanged and not affected by RMPs, the profiles with $\Delta\phi = 45°$ are more peaked than the standard ones. The T_e peaking factor, P_{T_e}, is here defined as the ratio between the electron temperature in the core and the averaged one in the region $R = 1.85 - 1.95$m; they are reported in Fig.10 for all the analyzed discharges as function of the final RE beam current I_{RE} (a) and of the RMP phasing applied (b). A slight decreasing trend can be observed between the peaking factor and I_{RE}; despite a large dispersion in the middle region, most peaked profiles with $P_{T_e} > 3.5$ correspond to lower I_{RE} and the other way around when $P_{T_e} < 3$. Such a dependence is more evident in panel (b), where the dashed line corresponds to the averaged peaking factor for shots without perturbations. For the less efficient perturbations, $\Delta\phi = 180°$ and $\Delta\phi = 270°$, the peaking factor is around $2.8 - 3$ the same of standard discharges; on the contrary P_{T_e} increases between $\Delta\phi = 0°$ and $90°$ even if with a larger dispersion for this latter value.

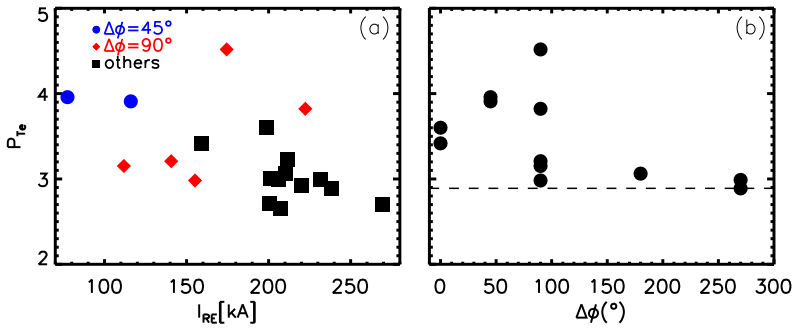

FIG. 10: Electron temperature peaking factor as function of the final post-disruption current (a) and of the phasing (b).

Thus, the peaking of the electron temperature profile appears to be correlated not only to specific phasing of the perturbations but also with their efficiency in reducing the RE post-disruption current. Such a decrease of temperature, which might be due to a partial degradation of the confinement properties, corresponds to a local growth of the collisionality which could affect also the primary generated runaways thus reducing the initial seed required for the avalanche mechanisms.

VI. EFFECT OF RMPS ON HXR ENERGY SPECTRUM.

The hard-X-ray radiation emitted by the runaways has been detected by a $LaBr_3(Ce)$ spectrometer with a counting rate capability up to MHz and high energy resolution (3% at 667keV) [46]. The variations in the HXR spectrum qualitatively reflect the changes in the RE energy distribution. A more detailed determination of the RE energy requires dedicated methods [47] and modeling activity is currently in progress. Four examples of HXR spectra, normalized to the total number of events, are reported in Fig.11 in the time interval between 1 and 1.05s (just after the disruption): the black curve refers to a standard discharge (no RMP applied), while the orange, red and blue ones to perturbed shots with $\Delta\phi = 0°, 45°, 90°$ phasing respectively. By analyzing the slope of these distributions it is found that the 45° trace falls off clearly faster in the range $300 - 800$ keV, with the exception of a quasi constant region between 400 and 500 keV which is of comparable shape also in the 90° discharge. On the other side, no significant differences in the HXR spectrum between the unperturbed and the $\Delta\phi = 0°$ shot are observed, both display an increased high energy content with respect to the other two discharges.

Three more examples are reported in Fig.12: the normalized HXR spectra of shots with $\Delta\phi =$

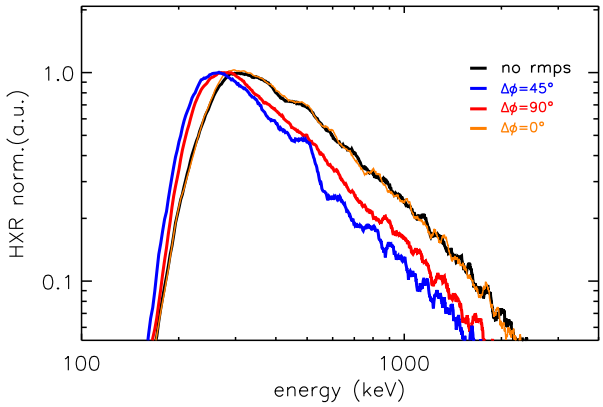

FIG. 11: (a): HXR energy spectrum from $LaBr_3(Ce)$ scintillator diagnostic for standard shot (black,#33505) and for three with RMPs applied but with different $\Delta\phi$ (45°-blue curve #33506 , 90°- red curve #33112, 0°- orange curve #33109).

$45°, 90°$ and without perturbations are evaluated in two different time interval: just after the disruption ($1 - 1.05s$, dashed line) and between $1.05s$ and $1.1s$ (c). For each spectrum and time interval, the average slope on the right of the peak has been evaluated by a power fit ($\propto E^{-\alpha}$) to quantify the effect of perturbations in reducing the high energy components of HXR distributions. For the case without RMPs a significant variation of α is not observed between the two time intervals, increasing from $\alpha = 1.3$ (for $1 < t < 1.05s$) to $\alpha = 1.5$ (between $1.05 < t < 1.1s$). A partially stronger effect is found when $\Delta\phi = 90°$ with α growing from 1.4 to 1.8 but the greatest variation is the one relative to the shot with $\Delta\phi = 45°$ where the slope becomes steeper by $\sim 60\%$ in the latter time interval with α passing from an initial values of 1.7 to 2.4. Such a result is of great relevance since it highlights a possible effect of the RMPs also during the RE beam phase.

A more detailed analysis on the time evolution of the HXR spectra is presented in Fig.13 where the coefficient α has been evaluated for the whole database of shots considered in this paper, in three time intervals ($1 - 1.05s, 1.05 - 1.1, 1.1 - 1.15s$) and in two different energy ranges (lower: $300 - 800$keV, higher : > 800keV). The results have been plotted both as function of the averaged RE current in the selected temporal intervals (a)-(b) and of the phasing of the applied perturbations. Panel (a) clearly shows that at lower energies, below 800 keV, the slope of the spectra scale with the current of the RE beam decreasing from $\sim 2 - 2.5$ at $I_{RE} \sim 50$kA to ~ 1 more typical of initial post-disruption current ($I_{RE} \sim 200$kA). The same behavior is not observed for high energies in panel (b) where α range between 2 and 8 but without a clear trend; nevertheless higher values of α, at least greater than 4.5 are found only at lower $< I_{RE} >$, thus in a later phase

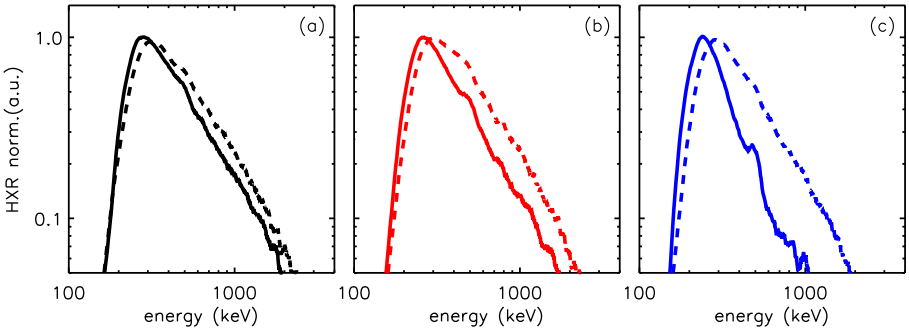

FIG. 12: HXR energy spectra reconstruction in two different time intervals after the disruption for shots without (panel (a),shot #33505) and with RMPs applied (90°-(b) #33658 and 45°-(c) #33706). The dashed line corresponds to the time interval $1 - 1.05s$ while the solid one to $1.05 - 1.1s$.

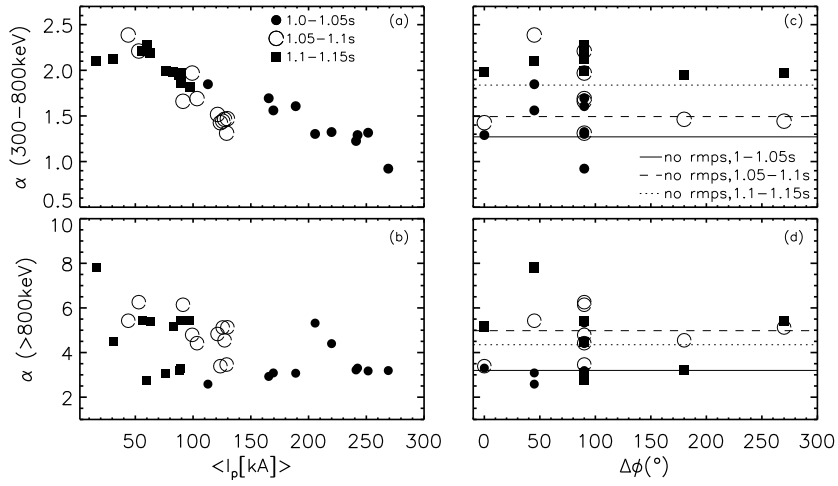

FIG. 13: (a): Slope of HXR energy spectrum from in the energy range $300 - 800$ keV and (b) > 800keV as function of the average current in different time intervals. (c)-(d): Same data but plotted versus the B-coil phasing.

of the beam evolution or when most efficient RMPs are applied.

The α evolution for different phasing of the perturbations is displayed in panel (c) and (d). The horizontal lines correspond to the average α for shots without perturbations (continuous for

$1-1.05s$, dashed for $1.05-1.1s$ and dotted for $1.1-1.15s$). At lower energies (panel (c)) an increase of α in time occurs for all the shots considered but the highest increase is relative to those with $\Delta\phi = 45°$. A large dispersion appears for $\Delta\phi = 90°$ characterized by values also below the ones of unperturbed shots. At higher energy (panel (d)), as for the RE current, a clear difference between shots with perturbations and without is difficult to be appreciated; the only exception is again represented by one discharge with $\Delta\phi = 45°$, that, in the third time interval considered ($1.1-1.15s$), is characterized by a very high α, close to 8.

A deeper and detailed understanding of the relation between the HXR energy spectrum and the corresponding runaway current requires an appropriate modeling of the RE physics which is beyond the scope of this paper. The data reported here show that most efficient RMPs act in order to reduce the post-disruption current which, in turn, is associated to steeper HXR spectra but with a strength depending on the energy ranges considered.

VII. ROLE OF PLASMA RESPONSE IN RE MITIGATION

The distinctive behavior of the phase $\Delta\phi = 45°$ with respect to others, as analyzed in the previous sections in relation to several quantities, will be discussed in this Section. The poloidal spectrum of the applied 3D fields has been evaluated in vacuum approximation at the time $t = 0.98$s, just before the disruption event, for more differential phases of the B-coils. Panels on the top of Fig.14 show the perturbed field as function of the poloidal wave number m and of the normalized poloidal flux coordinate ($\rho_{\rm pol}$) for $\Delta\phi = 0, 45°, 90°, 135°, 270°, 315°$, respectively. The safety factor profile is plotted with a white dashed line. The $\Delta\phi = 45°$ case shows that the maximum perturbed field occurs in the edge region and between the non-resonant component $m = 5$ and $m = 6$; the resonant position with $q = 4$ on the other hand lies in a region of low field (< 1.5 G). By increasing the B-coil phase difference, such a maximum is continuously shifted to lower values of m and at $\Delta\phi = 315°$ intersects the q profile and in particular the rational surfaces $q = 3$ and $q = 4$. As the parameter to quantify the variation of the RMP amplitude b_r with $\Delta\phi$, the value of the $m = 4$ perturbed field component at the resonance $q = 4$ was evaluated and shown in Fig.15(a) with a black-dashed line. As clear from this plot, the $n = 1$ radial field resonant with $q = 4$ (in the vacuum approximation) is maximum when $\Delta\phi \sim 315°$ with a minimum value close to zero around $\Delta\phi \sim 100°$; a similar trend is found also for the $m = 3$ mode estimated at $q = 3$ position (not shown in the figure for the sake of clarity). Such a dependence cannot explain the experimental data described in the previous sections summarized in Fig.15-(b)-(c) showing the

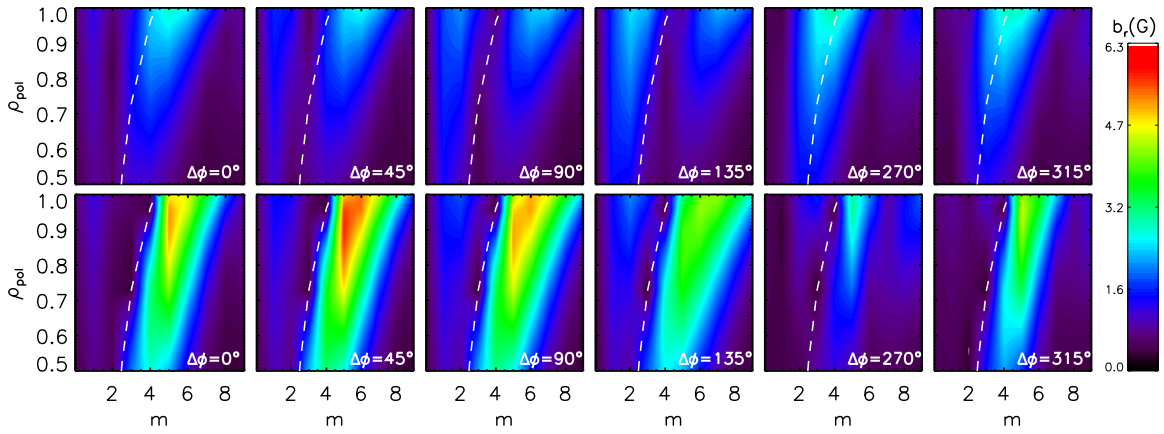

FIG. 14: Contour of perturbed field as function of the m component and normalized poloidal flux in vacuum approximation (top panels) and including the plasma response as computed by the code MARS-F (bottom panels) for the shot #33113 at 0.98s.

initial RE beam post-disruption current and its lifetime (the latter evaluated as the time from the current quench until I_{RE} drops below 10kA). Here, each point corresponds to a different discharge and the dashed line to the average post-disruption current for shots where RMPs are not applied. As already observed below, in the two shots with $\Delta\phi = 45°$ the initial runaway electron beam current is reduced by more than a factor of 2. A similar effect is found when $\Delta\phi = 90°$. No RE mitigation is observed for $\Delta\phi \sim 315°$ where RMPs give the largest vacuum contribution to the rational surface $q = 4$ (or $q = 3$).

The code MARS-F [48, 49], which solves the single-fluid linearly perturbed MHD equations in full toroidal geometry, has been used to calculate the poloidal spectrum including the plasma response to RMPs. Bottom panels in Fig.14 show the results obtained relative to an equilibrium preceding the disruption (reference shot: 33113, $t = 0.98$ s, the same used for the vacuum field reconstruction); the corresponding kinetic quantities such as electron/ion temperature and density profiles are provided to the code by Integrated Data Analysis (IDA) [50] of diagnostics. In these simulations a toroidal rotation of $\omega/\omega_A = 5 \cdot 10^{-3}$ is assumed (ω_A is the Alfvén frequency for these plasmas). At all values of the differential phase considered, the plasma response reduces the amplitude of resonant harmonics at the corresponding rational surfaces compared with the vacuum field; on the other hand the kink relative to the components $m = 5, 6$ for $\Delta\phi = 45°$ is enhanced by more than a factor 3. The same analysis has been performed for more $\Delta\phi$ and toroidal rotation values.

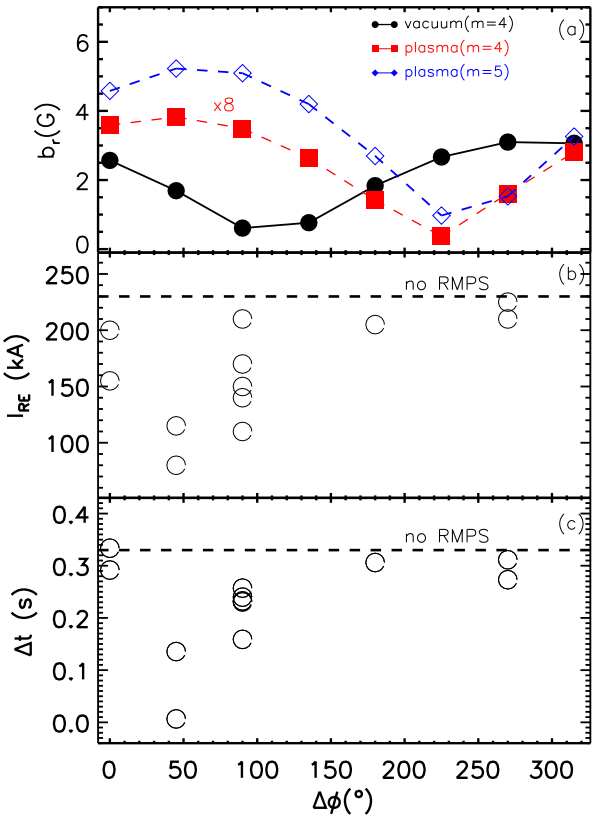

FIG. 15: (a) Perturbed field amplitude at the resonance $q = 4$ and of the kink mode $m = 5$ in the edge region, (b) post-disruption RE current and (c) lifetime. The dotted line corresponds to the average RE current in standard discharges.

As for the vacuum field, the $m = 4$ resonant component at $q = 4$ is shown in Fig.15-(a) with red squares; its amplitude is reduced by a factor ~ 8 with respect to the vacuum approximation. The differential phase relative to the maximum is shifted by $\sim 45° - 60°$ in the direction of increasing $\Delta\phi$ values, thus closer to the B-coil differential phase experimentally more successful in reducing the RE beam current. The same panel reports also the average amplitude of the non resonant mode $m = 5$ (blue-diamonds curve) in the edge region ($\rho_{pol} > 0.8$). A clear maximum can be observed at $\Delta\phi \sim 45° - 90°$ with an absolute value higher than 5 G; the RMP configuration for which runaway electrons are best mitigated is thus related to the largest edge kink response. A similar behavior was found for the B-coil configuration most efficient in suppressing edge localized modes (ELMs) [51, 52], where the maximum field evaluated including the plasma response is offset $\sim 60°$ from the one in vacuum approximation [53]. The results presented here, in particular

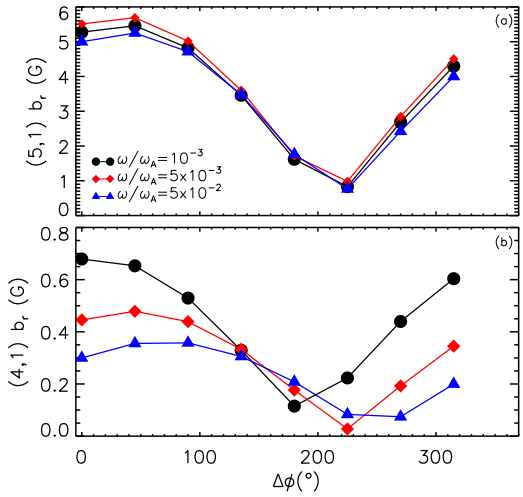

FIG. 16: (a) Perturbed field amplitude for the kink mode $n = 5$ in the edge region (a), and at the resonance position $(4, 1)$ (b) at different plasma rotations.

the dependence of the maximum b_r vs $\Delta\phi$, do not vary significantly with the toroidal rotation as can be observed in Fig.16. Panel (a) shows the average $m = 5$ component at the edge for ω/ω_A increasing from 10^{-3} to $5 \cdot 10^{-2}$; the curves are very close one each other and present the maximum value around 45°. The same analysis but for the $(4, 1)$ resonance is reported in panel (b); at larger rotation velocity, the plasma is more shielded from the penetration of external field and the resonant component is reduced. The phasing corresponding to the maximum perturbed field at the $(4, 1)$ resonance increases with rotation from $0° - 45°$ to $45° - 90°$. An estimate of the experimental toroidal flow can be inferred from the rotation frequency of the inner $(1, 1)$ mode when present and is of the order of ~ 5 kHz ($\omega/\omega_A \sim 2 - 3 \cdot 10^{-3}$); thus the experimental data analyzed in this paper correspond to an intermediate position between the black (circles) and red (squared) curves.

The total perturbed field (vacuum + plasma response) of the resonant field components is relevant in the formation of magnetic islands (e.g. harmonics $(4, 1)$ and $(3, 1)$) and, potentially, can be responsible for field line ergodization. But also the non-resonant part (kink amplification), that does not necessarily ergodize fields, further contributes to RE suppression (by coupling to resonant spectrum or direct orbit modification). In this sense, the combined results reported in Figure 14-15 point to two mechanisms both occurring at the same favorable coil phasing

which could affect the primary generated runaway electrons, thus reducing the initial seed, or those produced in the avalanche process. Nevertheless, a deeper understanding of these issues would require a detailed analysis directly by modeling the RE trajectories in these 3D fields [54] and/or an investigation with a two-fluid approach [55], considering also non-linear effects in the plasma response to RMPs. When two-fluid terms are included in the response calculations, the ion and electron rotation velocities are no longer the same; in particular the electron velocity results to be the relevant quantity controlling the field penetration in the core of the plasma at the mode-rational surface. Conversely, the excitation of edge modes is mainly correlated with the ion velocity [56]. Such an analysis might contribute to determine the necessary and sufficient conditions for the development of magnetic islands and of stochasticity.

VIII. RMPS APPLIED WITH LOWER AMPLITUDE AND IN THE POST-DISRUPTION PHASE

The impact of different amplitude of RMPs applied before the disruption with the most efficient phasing ($\Delta\phi = 45°$) has also been investigated. This has been done both by decreasing the current in the B-coils or keeping the maximum value available and varying the time at which they are switched on; indeed in this latter case, due to the slow diffusion time in the plasma, the perturbed field at the disruption is only a fraction of its final maximum value. Examples are reported in Fig.18-(b) showing one shot with $I_B = 0.8$kA from $t = 0.5$s (blue solid) and two with $I_B = 1$kA from $t = 0.8$s (solid orange and red lines); as references, also an unperturbed discharge is reported (black) and one with $I_B = 1$kA from $t = 0.5$s (dashed blue line). Despite slightly lower, the post-disruption RE current for shots with RMPs of reduced amplitude is very close to the one of the discharge without perturbations. Nevertheless the solid blue line ($I_B = 0.8$kA from $t = 0.5s$) is characterized by a faster decay of the RE beam with respect to the others and is more similar to that of the dashed line (full amplitude RMPs from $t = 0.5$s). These results highlight that a B-coil current of 1kA is probably close to the minimum threshold required to see any effect on the runaways. Such a finding is still in agreement with the plasma response modeling presented in the previous section as illustrated in Fig.17. Panel(a) shows again the radial field associated to the $m = 5$ component computed by MARS-F as function of the phasing; the maximum value at $\Delta\phi = 45°$ is of ~ 5.5G. Shots with RMP of reduced amplitude or with a delay of their application correspond to a different radial field associated. In the examples reported in Fig.18-(b), the blue

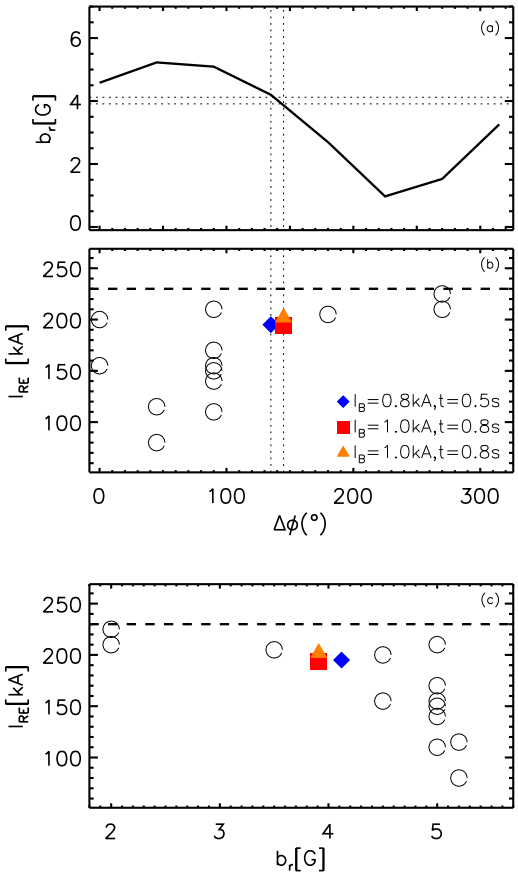

FIG. 17: (a) $m = 5$ perturbed field evaluated by MARS-F and (b) post-disruption current vs $\Delta\phi$ with included also the shots with different RMP amplitude and timing (square,triangle, diamond). (c) Post-disruption current vs the corresponding $m = 5$ perturbed field computed by MARS-F.

curve and the orange/red ones correspond to an effective field of 72% and 65% with respect to the maximum available; in panel (a) of Fig.17 the corresponding b_r values are indicated with dotted lines. Panel (b) of the same figure shows the post-disruption RE current as function of $\Delta\phi$ for discharges with the maximum (empty circles) and reduced (full symbols) RMPs amplitude. The latter data, as highlighted by the vertical dotted lines, are still in the trend traced out by the empty symbols; the reduced amplitude of the applied perturbation is equivalent to a radial field for the $m = 5$ kink mode generated by a different phasing (between 90° and 180° in these cases) with $I_B = 1$kA and starting time $t = 0.5$s. Panel (c) shows a combination of the other two panels, I_{RE} vs the $m = 5$ radial field applied by the B-coils as evaluated by MARS-F; within some dispersion a decreasing trend is observed. Moreover this latter plot also clarifies that a very narrow region in b_r is available to mitigate the post-disruption generated runaways. A larger

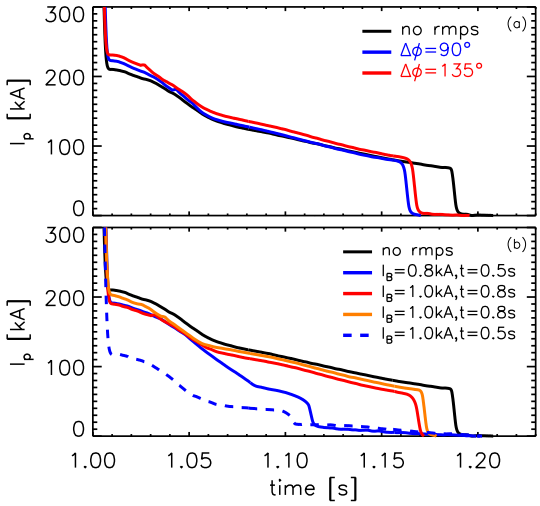

FIG. 18: (a) Examples of discharges with RMPs applied from $t = 1s$ (black-#34150, blue-#34143, red-#34144); (b) $\Delta\phi = 45°$ RMPs with different time of application and amplitude (black-#34150 reference shot without RMPs, blue solid-#34083, red-#34145 orange-#34146, blue-dashed: #33706-I_B = 1kA from $t = 1$s).

current in the B-coil might further reduce the runaway current and potentially increase the $\Delta\phi$ range useful in RE mitigation.

The results and considerations reported up to here refer to experiments with perturbations applied from a time preceding the disruptions, when plasmas are characterized by β values significantly greater than zero. On the contrary, post-disruption RE beams are generally almost cold plasmas with reduced minor and major radius as was shown in Fig.2. In these cases, a plasma response mechanism can be neglected and a vacuum approximation - while analyzing the effects of applied perturbations on runaways - is still adequate. In order to verify if RE mitigation occurs also with RMPs applied only once the RE beam is fully developed, few shots have been executed turning on the B-coils at $t = 1$s. By this choice RMPs do not interfere with the disruption dynamic since at least $200 - 300$ms are required for the fields to diffuse in the plasma core, as shown in Section III. A preliminary estimate of the phasing which could mostly affect the RE beam in the post-disruption phase is more difficult since the equilibrium is not stationary. Vacuum field reconstruction at several times show that, at least up to 1.2s, the differential phases between 50° and 150° maximize the RMPs components at the resonance positions closer to the edge. For

this reason perturbations with $\Delta\phi$ equal to 90° and 135° from $t = 1s$ have been applied; these shots are reported in Fig.18-(a) together with an unperturbed discharge belonging to the same experimental session. The evolution of RE current is rather similar for the three shots; the small variation in the initial current is not to be correlated with the effect of perturbations since their amplitude at $t \simeq 1$s inside the plasma is almost zero. Unfortunately, these shots are characterized by a fast loss of equilibrium between 1.15s and 1.2s thus much before the typical duration of the RE beam. On the other side, up to $t = 1.2$s the applied fields have not still completely built up in the plasma so it is not straightforward to conclude from these experiments if RMPs can affect an already developed RE beam or totally exclude this possibility.

IX. CONCLUSIONS.

The threat of post-disruption generated runaway electrons to in-vessel and plasma facing components in fusion devices requires the development of appropriate mitigation techniques. In ASDEX Upgrade a scenario dedicated to investigate methods which allow reducing the negative effects associated to runaway electrons has been established; a disruption is induced by argon puffing in a circular 0.8MA plasma followed by the generation of a runaway beam with an initial current of $200 - 300$kA and a duration up to 0.5s. Resonant magnetic perturbations have been applied by the B-coils with the maximum current available (1kA) and turned on 0.5s before the disruption. Experiments show that these perturbations significantly reduce the current and the lifetime of the generated RE beam. These findings are strongly dependent on the poloidal spectrum of the applied RMPs when the plasma response is included in the analysis by the code MARS-F. Indeed, the modest amplification (factor of $2 - 3$) of the edge kink response, with respect to a crude vacuum approximation, has to be considered to explain the phase dependence of the observed suppression effects. The most performing poloidal spectrum affects also the HXR spectrum characterized by a partial decrease of the energy content below 1MeV and the pre-disruptive electron temperature profile which is reduced by about $\sim 30\%$ in the region between $R = 1.8$m and $R = 2$m. Moreover also the current quench and RE beam decay phases are generally shortened when the most efficient perturbations are applied, suggesting their role in a worsening of the confinement properties. The application of RMPs before the disruption partially increases the density, probably because of an enhanced plasma-wall interaction. Nevertheless this effect on density occurs regardless of the RMP poloidal spectrum applied and of post-disruption current, thus is not directly correlated with the

observed RE mitigation.

Reduced amplitude RMPs, still applied from a time preceding the disruption, only marginally affect the initial runaway current but still in agreement with the plasma response modeling presented here; indeed the maximum current available for the B-coils in these experiments is found to be very close to the minimum threshold required to have any significant effect on the runaway beam. Perturbation applied after the disruption do not seem to affect the RE beam evolution but the recurring loss of RE beam position control in these experiments prevents to draw definitive conclusions on this issue, since the fields - due to the surrounding conductive structures - might require times longer than 200ms to penetrate the plasma.

These results can contribute to explain similar experiments performed in other tokamak devices and - combined with disruption predictive models and in synergy with standard mitigation methods - be relevant for RE suppression in future fusion reactors.

Acknowledgments. A special thanks to R.Fischer for providing us the inputs data for MARS-F simulations. This work has been carried out within the framework of the EUROfusion Consortium and has received funding from the Euratom research and training programme 2014-2018 under grant agreement No 633053. The views and opinions expressed herein do not necessarily reflect those of the European Commission. Work supported by US DoE Office of Science under Contract DE-FG02- 95ER54309 and DE-FC02-04ER54698.

---

[1] The ITER physics basis. Nucl. Fusion **47**, S1-S413 (2007).

[2] Hender T. C. *et al.* Nucl. Fusion **47**, S128202 (2007)

[3] E.C.Hollmann *et al.* Phys.Plasmas **22**, 056108 (2015)

[4] M. Lehnen *et al.* JNM **463** 39 (2015)

[5] R.S.Granetz *et al.* Phys. Plasmas **21** , 072506 (2014)

[6] M.N.Rosenbluth and S.V.Putvinski, Nucl.Fusion **37**, 1355 (1997)

[7] J. W. Connor and R. J. Hastie, Nucl. Fusion **15**, 415424 (1975)

[8] R.Aymar, *et al*, Plasma Phys. Control. Fusion **44**, 519 (2002)

[9] Hender T.C. *et al.* , The ITPA MHD, Disruption and Magnetic Control Topical Group 2007 Nucl. Fusion **47** S128

[10] A.H.Boozer Nucl. Fusion **57**, 056018 (2017)

[11] G.Papp *et al.* Plasma Physics and Controlled Fusion, **54** (2012)

[12] M. Lehnen *et al.* Journal of Nuclear Materials **463** 3948 (2015)

[13] Eidietis N W *et al* Phys. Plasmas **19** 056109 (2012)

[14] B.Esposito *et al* Plasma Phys. Control. Fusion **59** 014044 (2017)

[15] Bakhtiari M. *et al* Nucl. Fusion **42**, 1197 (2002)

[16] S. A. Bozhenkov *et al* Plasma Phys. Control. Fusion **50**, 105007 (2008)

[17] C.Reux *et al*, Nucl. Fusion **50**, 095006 (2010)

[18] Z. Y. Chen, Plasma Phys. Control. Fusion **55**, 014046 (2017)

[19] G.Pautasso *et al*, Plasma Phys. Control. Fusion **59**, 035007 (2016)

[20] M. Lehnen *et al* Nucl. Fusion **53** (9), 093007 (2013)

[21] Taylor P.L. *et al* Phys. Plasmas **6**, 1872 (1999)

[22] N.Commaux *et al* Nucl. Fusion **56** 046007 (2016)

[23] G.M.Olynyk *et al* Nucl. Fusion **53** 092001 (2013)

[24] P.Helander *et al* Phys.Plasmas **7**, 4106 (2000)

[25] R.W.Harvey *et al*, Phys. Plasmas **7**, 4590 (2000)

[26] M.Lehnen *et al*, Phys.Rev.Lett. **100**, 255003 (2008)

[27] K. Wongrach1 *et al* Nucl. Fusion **55**, 053008 (2015)

[28] Hollmann E.M. *et al* Phys. Plasmas **17** 056117 (2010)

[29] R.Yoshino *et al*, Nucl.Fusion **40**, 1293 (2000)

[30] M.Gobbin *et al.* Nucl. Fusion **57**, 016014 (2017)

[31] G.Papp *et al.* Journal of Plasma Physics **81** 47581050 (2015)

[32] K.Aleynikova *et al.*, P. Plasma Phys. Rep. **42**, 486 (2016)

[33] T.Evans *et al.*, Phys. Rev. Lett. **92**, 235003 (2004)

[34] M.Gobbin *et al.* submitted to Phys. Rev. Lett.

[35] A.Kallebanch *et al.* to be published on Nuclear Fusion (IAEA 2016)

[36] W.Suttrop *et al.*. Phys. Rev. Lett. **106** 225004 (2011)

[37] Y.Q.Liu *et al.* Nucl. Fusion **51** (2011)

[38] G.Papp *et al.* to be published in Nuclear Fusion (IAEA 2016)

[39] M.Nocente *et al* Rev. Sci. Instrum. **81**, 10D321 (2010)

[40] M.Nocente *et al* IEEE Trans. Nucl. Sci. **60** 1408 (2013)

[41] G. A. Rattá, *et al.*, Nuclear Fusion **50** 025005 (2010)

[42] G.Pautasso *et al.*, Nuclear Fusion **51** 103009 (2011).

[43] S. Dormido-Canto *et al.*, Nuclear Fusion **53** 113001 (2013).

[44] P. De Vries *et al* Nuclear Fusion **56** 2 (2016)

[45] N.Commaux *et al.* Nucl. Fusion **51**, 103001 (2011)

[46] M. Nocente *et al.* Nucl. Fusion **57** 076016 (2017)

[47] A.E. Shevelev *et al* Nucl. Fusion **53** (2013) 123004

[48] Y.Q.Liu *et al.* Phys. Plasmas **7** 3681 (2000)

[49] Y.Q.Liu *et al.* Phys. Plasmas **17** 122502 (2010)

[50] R.Fischer *et al.* Fusion Sci. Technol.**58** 675 (2010)

[51] F.Orain *et al.* Nucl. Fusion **57** 022013 (2017)

[52] L.Li *et al.* Nucl. Fusion **56**, 126007 (2016)

[53] D.A.Ryan *et al.* Plasma Phys. Control. Fusion **57** 095008 (2015)

[54] K. Sarkimaki *et al.* Plasma Phys. Control. Fusion **58** 125017 (2016)

[55] F.Orain *et al.* 2013 Physics of Plasmas **20**, 102510 (2013)

[56] N.M. Ferraro, Phys.Plasmas **19**, 056105 (2012)